Heliyon 10 (2024) e26858

Contents lists available at ScienceDirect

Heliyon

journal homepage: www.cell.com/heliyon

Research article

# Slow blood-flow in the left atrial appendage is associated with stroke in atrial fibrillation patients

Nikhil Paliwal [a,1], Hwan-Cheol Park [b,1], Yuncong Mao [c], Su Jin Hong [d], Yonggu Lee [b], David D. Spragg [e], Hugh Calkins [e], Natalia A. Trayanova [a,f,g,*]

[a] Alliance for Cardiovascular Diagnostic and Treatment Innovation, Johns Hopkins University, Baltimore, MD, USA
[b] Division of Cardiology, Department of Internal Medicine, Hanyang University College of Medicine, Guri City, Republic of Korea
[c] Department of Neuroscience, Johns Hopkins University, Baltimore, MD, USA
[d] Department of Radiology, Hanyang University Guri Hospital, Hanyang University College of Medicine, Republic of Korea
[e] Division of Cardiology, Department of Medicine, Johns Hopkins University School of Medicine, Baltimore, MD, USA
[f] Department of Medicine, Johns Hopkins University School of Medicine, Baltimore, MD, USA
[g] Department of Biomedical Engineering, Johns Hopkins University, Baltimore, MD, USA

ARTICLE INFO

*Keywords:*
Atrial fibrillation
Stroke
Hemodynamics
Patient-specific simulation
Computational fluid dynamics

ABSTRACT

*Background:* Atrial fibrillation (AF) patients are at high risk of stroke with ~90% clots originating from the left atrial appendage (LAA). Clinical understanding of blood-flow based parameters and their potential association with stroke for AF patients remains poorly understood. We hypothesize that slow blood-flow either in the LA or the LAA could lead to the formation of blood clots and is associated with stroke for AF patients.

*Methods:* We retrospectively collected cardiac CT images of paroxysmal AF patients and dichotomized them based on clinical event of previous embolic event into stroke and non-stroke groups. After image segmentation to obtain 3D LA geometry, patient-specific blood-flow analysis was performed to model LA hemodynamics. In terms of geometry, we calculated area of the pulmonary veins (PVs), mitral valve, LA and LAA, orifice area of LAA and volumes of LA and LAA and classified LAA morphologies. For hemodynamic assessment, we quantified blood flow velocity, wall shear stress (WSS, blood-friction on LA wall), oscillatory shear index (OSI, directional change of WSS) and endothelial cell activation potential (ECAP, ratio of OSI and WSS quantifying slow and oscillatory flow) in the LA as well as the LAA. Statistical analysis was performed to compare the parameters between the groups.

*Results:* Twenty-seven patients were included in the stroke and 28 in the non-stroke group. Examining geometrical parameters, area of left inferior PV was found to be significantly higher in the stroke group as compared to non-stroke group ($p = 0.026$). In terms of hemodynamics, stroke group had significantly lower blood velocity ($p = 0.027$), WSS ($p = 0.018$) and higher ECAP ($p = 0.032$) in the LAA as compared to non-stroke group. However, LAA morphologic type did not differ between the two groups. This suggests that stroke patients had significantly slow and oscillatory circulating blood-flow in the LAA, which might expose it to potential thrombogenesis.

*Conclusion:* Slow flow in the LAA alone was associated with stroke in this paroxysmal AF cohort. Patient-specific blood-flow analysis can potentially identify such hemodynamic conditions, aiding in clinical stroke risk stratification of AF patients.

* Corresponding author. Hackerman 216, 3400 N Charles St, Baltimore, MD 21218, USA.
*E-mail address:* ntrayanova@jhu.edu (N.A. Trayanova).
[1] Equal contributions.

https://doi.org/10.1016/j.heliyon.2024.e26858
Received 5 April 2023; Received in revised form 16 February 2024; Accepted 21 February 2024
Available online 28 February 2024
2405-8440/© 2024 The Authors. Published by Elsevier Ltd. This is an open access article under the CC BY-NC license (http://creativecommons.org/licenses/by-nc/4.0/).

## 1. Introduction

Atrial fibrillation (AF) is the most common form of arrhythmia that causes high mortality rate due to dramatically increased stroke risk [1]. For managing stroke risk in AF patients, their clinical and demographic characteristics are used to identify their candidacy for oral anticoagulation therapy [2]. The most commonly used is the $CHA_2DS_2$-VASc score, which scores patients based on their age, sex, congestive heart failure, hypertension, prior stroke, vascular disease and diabetes history [3]. $CHA_2DS_2$-VASc has demonstrated moderate performance in predicting stroke risk for AF patients, with stroke events ranging from ~1% for low-risk to ~6% in high-risk AF patients [4]. Additionally, $CHA_2DS_2$-VASc score also has sub-optimal performance in selected populations like patients with renal insufficiency and Asian patients [5]. An inherent limitation of such score is the lack of use of AF patients' atrial structural and anatomical factors in evaluating stroke risk [6].

It is well known that atria of patients with AF undergoes remodeling, altering atrial anatomy and function [7]. Studies have also shown that remodeled LA anatomy and function such as LA size, reservoir function and left atrium appendage (LAA) are associated with increased stroke for AF patients. However, the exact mechanisms by which the remodeled anatomy and function of LA and LAA contribute to stroke propensity in AF patients is currently unknown. Previous imaging and simulation-based blood-flow studies have explored potential relationship between slow flow and stroke/thrombosis [8–21]. Building upon this understanding, we hypothesize that low and oscillating blood-flow in either the remodeled LA or the LAA of AF patients is associated with potential clot formation, and

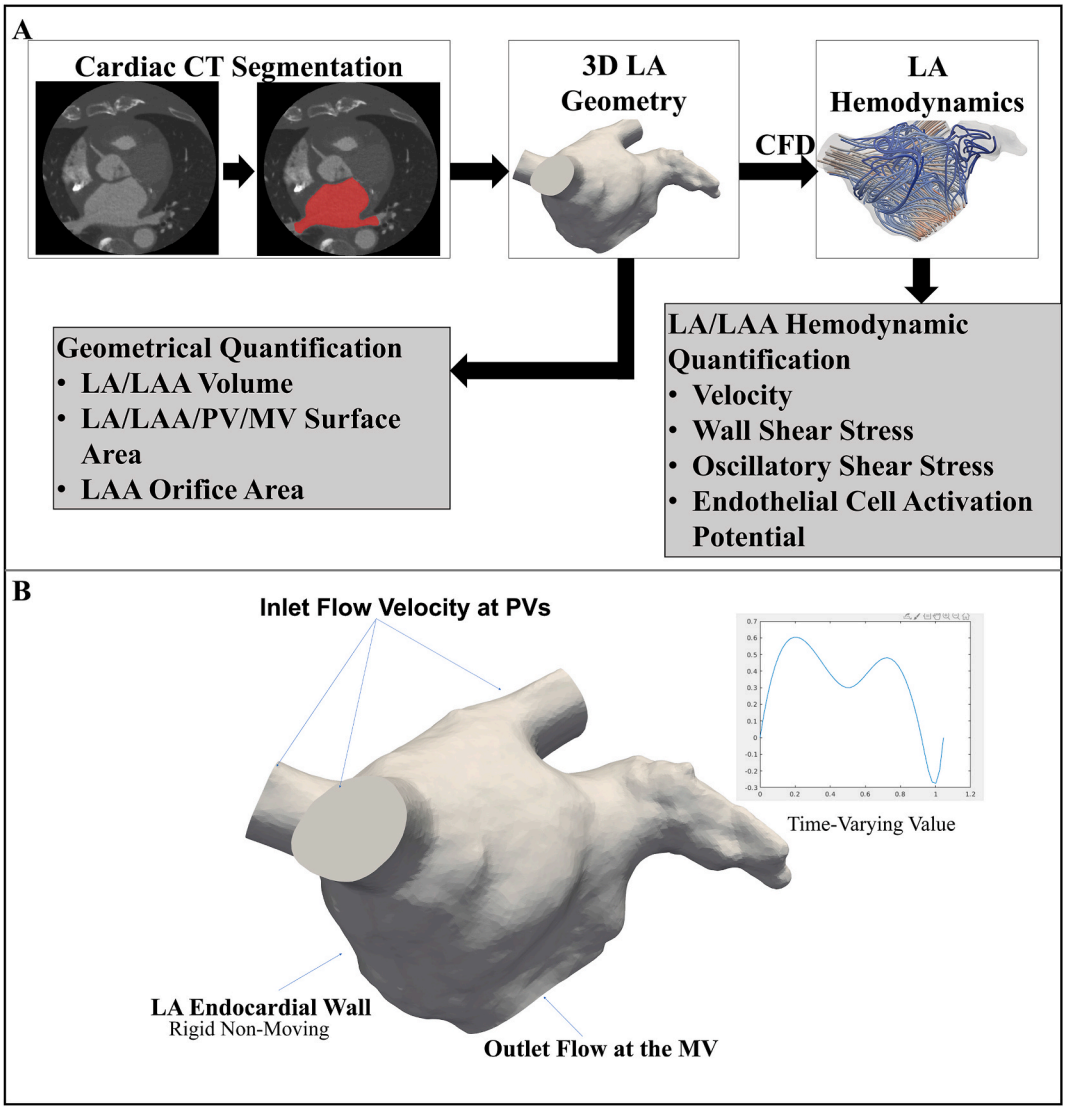


**Fig. 1.** A. Overview of the patient-specific left atrial and left atrial appendage geometrical and hemodynamic parameters assessment from cardiac CT imaging data of AF patients. Also included is the list of LA and LAA parameters obtained for each AF patient. B. Boundary conditions for the CFD simulations.

their eventual stroke risk. To test this hypothesis, we use patient-specific LA blood-flow modeling on patient-specific LAs of paroxysmal AF patients that had a clinical stroke event and compare with those of patients with no history of stroke to identify parameters that could be associated with stroke. Additionally, we also compare commonly calculated LA and LAA geometrical and morphological parameters between the two groups.

## 2. Materials and methods

We present an outline of the approach employed for the geometrical and hemodynamic assessment of the LA and LAA using clinical images. The methodology is described in Fig. 1, where panel 1A shows the geometrical and hemodynamic quantification, and panel 1B shows the blood-flow dynamics inlet and boundary conditions. Detailed explanation follows in subsequent sections.

### 2.1. Patient data acquisition and LA segmentation

We retrospectively collected clinical data and cardiac computed tomographic (CT) images of patients with paroxysmal AF that had a clinically documented embolic stroke event (including transient ischemic attack) and paroxysmal AF patients that did not have stroke event from Hanyang University Guri Hospital in Republic of Korea. From January 2018 to December 2019, patients with non-valvular paroxysmal AF who visited the cardiovascular center with various symptoms requesting cardiac multi-detector computerized tomography (MDCT) were enrolled consecutively in either group according to previous stroke event. Patients with valvular heart disease, prosthetic valves, and AF rhythm during MDCT images were excluded. MDCT was analyzed to evaluate the morphologic features of LAA, LA volume, LAA volume, and pulmonary veins anatomy. Cardiac MDCT was performed using a 128-slice dual source system (SOMATOM Definition Flash; Siemens Healthcare, Erlangen, Germany). To define the morphology of the LAA, three-dimensional reconstruction of the LA and LAA structures was performed with commercially available software (EnSite Verismo Segmentation Tool Software; St. Paul, Minnesota) [22]. Two investigators who were blinded to patient's clinical information classified the morphologic types of LAAs independently. When there was a disagreement between the 2 investigators' classification, the third investigator was involved to resolve the disagreement. LAA morphology was classified into the following four categories as previously described [23]: (1) chicken wing type, and obvious bend in the proximal or middle part of the dominant lobe; (2) cauliflower type, complex internal characteristics with the lack of a dominant lobe; (3) windsock type, a dominant lobe plus secondary or even tertiary lobes arising from the dominant lobe; and (4) cactus type, a dominant central lobe with small chambers extending in all directions. LA and LAA volumes in MDCT were measured using commercially available software (Aquaris iNtuition Viewer Version 4.4; TeraRecon, Foster City, California) [24]. LAA orifice diameters were also measured by previously described method [22]. Demographic characteristics, past medical histories, and social histories were obtained and also analyzed. Approval for the collection and review of patient clinical data was obtained from the local Institutional Review Board. For computational analysis, cardiac CT images were segmented using a semi-automated image-intensity thresholding method using ITK-snap (www.itksnap.org) [25] to obtain the 3D surface of the LA for each patient.

### 2.2. Left atrial geometrical assessment

Utilizing the segmented 3D LA geometry of each patient, various geometrical parameters were computed. These included surface area and volume of the LA, as well as surface area and volume of the LAA using Meshmixer (Autodesk Research, New York, NY). The LA geometry was partitioned to isolate the four pulmonary veins (PVs), mitral valve (MV), and LAA using open-source Computational Geometry Algorithms Library (www.cgal.org). This isolation was achieved using the shape diameter function (SDF) from a computational geometry library. The SDF calculated the local diameter at each point on the LA surface, enabling the identification of different parts of the LA based on local curvature. Geometrical parameters, such as PV area, MV area, LAA volume, LAA surface area, and LAA orifice area, were determined for each case.

### 2.3. Computational fluid dynamics methodology

Details of the patient-specific blood-flow modeling simulation tool can be found in the Supplementary Material and in previous studies [26–28]. In summary, the 3D model of the left atrium (LA) for each case was meshed using tetrahedral elements in the LA volume, with prism layers at the LA wall, employing ICEM CFD software (Ansys, Canonsburg, PA). The average element size was approximately 0.5 mm, resulting in approximately 3–10 million elements in each LA model, depending on its size. These mesh parameters were determined based on a mesh independence study, as described in the Supplementary Materials. The boundary conditions (BCs) were set with inlets at the four pulmonary veins (PVs) and a zero-velocity gradient outlet BC at the mitral valve (MV), assuming a rigid LA wall. To represent physiological blood flow at the PVs, Doppler-recorded velocity values obtained from the literature for AF patients were interpolated (Gentile et al., 1997; de Marchi et al., 2001). The blood was modeled as a Newtonian fluid with fixed density and viscosity values of 1056 $kg/m^3$ and 0.0035 Pa-s, respectively. The discretized Navier-Stokes equations were solved using the icoFoam module of the open-source OpenFOAM software, employing 1st order implicit temporal Euler discretization for time and 2nd order spatial linear discretization for space. The simulations were conducted for three identical cardiac cycles during sinus rhythm to ensure numerical stability, and the results from the third cycle were used as the simulation outcome. Each cardiac cycle had a length of 0.92 s, with a temporal resolution of 0.001 s [28]. The hemodynamic results were recorded at 92-time intervals for each case, representing the blood flow in the LA with a resolution of 0.01 s. The simulations were performed at the Maryland Advanced

Research Computing Center supercomputing facility. On average, one LA flow simulation took approximately 8 h to complete on an exclusive Intel Cascade Lake 6248R node with 48 cores and 192 GB RAM.

### 2.4. Left atrial hemodynamic assessment

For each case, the simulation results from the 92 solution points were exported to quantify four hemodynamic metrics defined over a single cardiac cycle in sinus rhythm. These metrics included time-averaged velocity, time-averaged wall shear stress (WSS), oscillatory shear index (OSI), and endothelial cell activation potential (ECAP). Time-averaged velocity represented the average blood velocity during sinus rhythm. WSS, OSI, and ECAP were derived from the frictional stress of the blood flow at the LA wall, providing information about the local blood flow patterns. All LA hemodynamic parameters were normalized before comparing two groups (stroke and non-stroke group). OSI was computed based on the difference in the direction of the WSS vector over a cardiac cycle, normalized by its magnitude (Xiang et al., 2011). OSI values ranged from 0 to 0.5, with 0.5 indicating a 180° change in the WSS vector direction during a cardiac cycle. ECAP was defined as the ratio of OSI to WSS and highlighted regions of low WSS and high OSI, representing areas of abnormal hemodynamics in vascular flows (Himburg et al., 2004; Chiu et al., 2003; Di Achille et al., 2014). Equations for calculations of these hemodynamic metrices can be found here [26] and were calculated using ParaView (https://www.paraview.org/) for both the LA and LAA for each case [29].

### 2.5. Data analysis and statistical methods

The operator performing the analysis of LA and LAA geometrical and hemodynamic parameters was blinded to the clinical stroke outcomes of the AF patients. The de-identified clinical images and analyzed data are available upon request and with appropriate institutional review board approval. Statistical analysis was conducted to compare the two patient groups.

For comparing the two groups, a one-sample Kolmogorov-Smirnov test was initially conducted to assess the normal distribution of each parameter. Subsequently, the Student t-test was employed to evaluate statistical differences between parameters with normal distribution, while the Mann-Whitney *U* test was used for non-normally distributed data. A p-value less than 0.05 was considered statistically significant. Normally distributed continuous variables were presented as mean ± standard deviation, whereas non-normally distributed continuous variables were reported as median [inter-quartile range]. The statistical analysis was performed using SPSS Statistics 22.0 software (IBM Corp., Armonk, NY, USA).

**Table 1**
Patient clinical, demographic and laboratory data information in the two groups. PLT: platelets, HTN: hypertension, DM: diabetes mellitus, CAD: coronary artery disease, HF: heart failure.

| | Non-stroke (n = 28) | Stroke (n = 27) | p value |
|---|---|---|---|
| Demographics | | | |
| Male Sex (%) | 15 (57.7) | 16 (59.3) | 0.910 |
| Age (Years) | 73.1 ± 5.1 | 72.3 ± 6.0 | 0.575 |
| Height (cm) | 160.97 ± 8.28 | 159 ± 9.17 | 0.415 |
| Weight (kg) | 65.17 ± 8.38 | 60.61 ± 10.64 | 0.089 |
| Anti PLT agents (%) | 15 (57.7) | 15 (55.6) | 0.878 |
| Anticoagulation (%) | 1 (3.8) | 0 (0) | 0.309 |
| Alcohol (%) | 5 (20) | 5 (18.5) | 0.895 |
| Smoking (%) | 1 (3.8) | 2 (7.4) | 0.585 |
| Comorbidities | | | |
| HTN (%) | 21 (80.8) | 20 (74.1) | 0.570 |
| DM (%) | 10 (38.5) | 15 (55.6) | 0.227 |
| Dyslipidemia (%) | 3 (11.5) | 7 (25.9) | 0.195 |
| CAD (%) | 22 (84.6) | 25 (92.6) | 0.373 |
| HF (%) | 16.0 (61.5) | 15.0 (55.6) | 0.666 |
| Vascular diseases (%) | 8.0 (30.8) | 8.0 (29.6) | 0.930 |
| $CHA_2DS_2$-VASc score (without stroke) | 4 [3,5] | 4 [3,5] | 0.547 |
| 0–1 | 1.0 (3.8) | 0.0 (0.0) | 0.245 |
| 2–3 | 6.0 (23.1) | 13.0 (48.1) | |
| 4–5 | 15.0 (57.7) | 11.0 (40.7) | |
| ≥6 | 4.0 (15.4) | 3.0 (11.1) | |
| Laboratory Data | | | |
| SBP (mmHg) | 121 [119.0, 138.5] | 135 [122.3, 150.0] | 0.084 |
| DBP (mmHg) | 70 [67.5, 80.0] | 70 [68.8, 80.0] | 0.475 |
| Glucose (mg/dL) | 102 [88.5, 127.0] | 122 [106.3, 162.3] | 0.011 |
| HbA1c (%) | 6.0 [5.6, 6.6] | 6.3 [6.1, 6.8] | 0.267 |
| Creatinine (mg/dL) | 0.91 [0.77, 1.07] | 0.88 [0.63, 1.19] | 0.832 |
| eGFR (mL/min/1.73m2) | 76.2 [58.3, 86.8] | 76.8 [62.1, 87.9] | 0.616 |
| Total Cholesterol (mg/dL) | 138 [129.5, 163.0] | 159 [130.0, 173.3] | 0.233 |
| TG (mg/dL) | 125 [97.0, 190.5] | 110.5 [80.0, 182.3] | 0.331 |
| LDL Cholesterol (mg/dL) | 78 [69.5, 99.0] | 89.5 [69.5, 113.0] | 0.418 |
| HDL Cholesterol (mg/dL) | 44 [41.5, 50.0] | 44 [38.8, 51.8] | 0.895 |

## 3. Results

### 3.1. Patient clinical and demographic information

Twenty-seven paroxysmal AF patients had a clinically confirmed ischemic stroke event and were included in the stroke group. Twenty-eight control paroxysmal AF patients who did not have stroke were included in the non-stroke group. Cardiac MDCT was performed in all patients. Patient demographic and clinical comorbidities of the two groups is listed in Table 1. Average age of patients was 72 [70, 75] years in the stroke group and 72 [67, 75] years in the non-stroke group. There was no statistically significant difference between the two groups in terms of their age and other clinical and demographic data as listed in Table 1. There was inevitable difference between the two groups in $CHA_2DS_2$-VASc score because the population of Stroke group had more 2 points than the other group automatically. Therefore, we analyzed the modified $CHA_2$D-VASc score to compare the two groups excluding the scores assigned for previous stroke events in the stroke group. There was no significant difference between the two groups in the $CHA_2$D-VASc score in Table 1. The incidences of anti-platelets agent use or anticoagulants including warfarin or NOAC were not different between the two groups.

### 3.2. Geometrical differences between stroke and non-stroke group

Differences in geometrical parameters between the two groups is listed in Table 2. In terms of LA geometry, there was non-significant difference between the LA area ($p = 0.717$) and volume ($p = 0.874$) between the groups, with the stroke group having smaller volume and area of the LA as compared to the non-stroke group. Among the four PVs, LSPV, RSPV and RIPV had larger area in the non-stroke group as compared to the stroke group, but these differences were non-significant (LSPV $p = 0.846$, RSPV $p = 0.362$, RIPV $p = 0.191$). However, LIPV was significantly smaller in the non-stroke group as compared to the stroke group ($p = 0.026$). MV area was similar among the two groups with insignificant difference ($p = 0.863$). None of the LAA geometrical parameters were significantly different between the stroke and non-stroke groups. Stroke group had bigger LAA, with higher values of both volume and area (LAA volume $p = 0.3232$, LAA surface area $p = 0.323$), while LAA orifice area was smaller in the stroke group ($p = 0.854$). We also characterized the LAA morphologies according to the 4 common clinical shape descriptors: chicken-wing, cactus, cauliflower and windsock.[20] The stroke group consisted of 4 (14.8%) chicken-wing, 10 (37%) cauliflower, 9 (33.3%) windsock and 4 (14.8%) cactus morphologies of the LAA. The non-stroke group had 10 (38.5%) chicken-wing, 8 (30.8%) cauliflower, 5 (19.2%) windsock and 3 (11.5%) cactus morphologies of the LAA. The morphologies of LAA were not significantly different between the two groups.

### 3.3. Hemodynamic differences between stroke and non-stroke group

In terms of LA hemodynamics, the stroke group had lower velocity and WSS but higher OSI and ECAP as compared to the non-stroke group, but these differences were not significant (Table 3, LA velocity $p = 0.495$, LA WSS $p = 0.292$, LA OSI $p = 0.380$, LA ECAP $p = 0.256$). However, for LAA hemodynamics, we found that velocity and WSS in the LAA were significantly lower ($p = 0.027$ and $p = 0.018$, respectively) and ECAP was significantly higher ($p = 0.032$) in the stroke-group as compared to the non-stroke group. Additionally, LAA OSI was also higher in the stroke group, but with non-significant difference from the non-stroke group ($p = 0.256$).

We plotted hemodynamic differences in four representative non-stroke and stroke patient's LA in Figs. 2 and 3, respectively. Each panel in both Figures represents time-averaged velocity magnitude streamlines, time-averaged WSS, OSI and ECAP, respectively with red dotted circle identifying the LAA for each case as the focus of hemodynamic interest. All 4 cases are examples of each type of LAA morphology as indicated on the side of each panel. As seen in Figs. 2 and 3, non-stroke cases (2A and 3A, respectively) had more

**Table 2**
LA and LAA geometrical parameters in the two groups. LA: left atrium, LAA: left atrium appendage, LSPV: left superior pulmonary vein, RSPV: right superior pulmonary vein, LIPV: left inferior pulmonary vein, RIPV: right inferior pulmonary vein, PV: pulmonary vein, MV: mitral valve.

| Geometrical Parameter | Non-Stroke (n = 28) | Stroke (n = 27) | p-value |
|---|---|---|---|
| LSPV Area ($mm^2$) | 209.5 [135.3, 244.3] | 172.7 [131.4, 249.8] | 0.854 |
| RSPV Area ($mm^2$) | 210.2 [175.2, 2.73.6] | 199.5 [178.2, 249.0] | 0.629 |
| LIPV Area ($mm^2$) | 119.0 [92.7, 146.8] | 160.7 [120.3, 180.2] | 0.021 |
| RIPV Area ($mm^2$) | 166.6 [134.8, 225.0] | 161.4 [121.7, 225.0] | 0.616 |
| Mean PA Area ($mm^2$) | 191.6 ± 50.0 | 192.6 ± 43.2 | 0.940 |
| MV Area ($mm^2$) | 902.4 ± 194.5 | 946.8 ± 297.3 | 0.531 |
| LA Area ($mm^2$) | 11093.5 ± 2140.1 | 11104.3 ± 2130.1 | 0.985 |
| LA Volume ($mm^3$) | 80000.8 [60656.6, 89235.1] | 72992.0 [61628.4, 87019.5] | 0.944 |
| LAA Volume (mm3) | 5192.7 [3763.5, 6824.8] | 5520.0 [4718.8, 7212.2] | 0.493 |
| LAA Surface Area Closed ($mm^2$) | 2164.6 [1653.6, 2388.3] | 2133.6 [1829.1, 2487.7] | 0.504 |
| LAA Orifice Area ($mm^2$) | 313.0 ± 111.4 | 316.6 ± 107.0 | 0.904 |
| Morphology (%) | | | 0.276 |
| 1 (Chicken wing) | 10 (38.5) | 4 (14.8) | 0.051 |
| 2 (Cauliflower) | 8 (30.8) | 10 (37) | 0.630 |
| 3 (Windsock) | 5 (19.2) | 9 (33.3) | 0.244 |
| 4 (Cactus) | 3 (11.5) | 4 (14.8) | 0.725 |

**Table 3**
Hemodynamic parameters in the two groups. LA: left atrium, WSS: wall shear stress, OSI: oscillatory shear index, ECAP: endothelial cell activation potential, LAA: left atrium appendage.

| Hemodynamic Parameter | Non-Stroke (n = 28) | Stroke (n = 27) | p-value |
|---|---|---|---|
| LA Velocity (m/s) | 0.24 [0.20, 0.29] | 0.22 [0.20, 0.27] | 0.713 |
| LA WSS (PA) | 0.0021 [0.0018, 0.0029] | 0.0020 [0.0017, 0.0026] | 0.562 |
| LA OSI | 0.084 [0.072, 0.113] | 0.096 [0.069, 0.114] | 0.585 |
| LA ECAP (1/PA) | 42.0 ± 21.1 | 46.5 ± 24.2 | 0.477 |
| LAA Velocity (m/s) | 0.079 [0.047, 0.116] | 0.050 [0.037, 0.077] | 0.043 |
| LAA WSS (PA) | 0.00065 [0.00036, 0.00106] | 0.00040 [0.00028, 0.00058] | 0.032 |
| LAA OSI | 0.10 ± 0.04 | 0.11 ± 0.04 | 0.193 |
| LAA ECAP (1/PA) | 109.3 [80.6, 294.0] | 259.5 [104.3, 437.3] | 0.040 |

velocity streamlines entering the LAA (within the red dotted region), which had lower number of streamlines going in, signifying lower blood-flow entering the LAA of representative stroke cases (2B and 3B, respectively) as compared to non-stroke cases. In terms of WSS, Figs. 2 and 3 again shows that both non-stroke cases had regions of both high WSS (red color on the LAA surface) as well as low WSS (blue color on the LAA surface), whereas for stroke cases, LAA was almost entirely blue in both cases showing lower WSS representing slower flow in representative stroke cases. In terms of OSI and ECAP, OSI was similar in the LAA's of all 4 cases both in Figs. 2 and 3, with regions of low OSI (black color on the LAA surface) dominating the flow, except for the stroke case with cauliflower morphology that had higher OSI (white color on the LAA surface). Same trends can be seen for ECAP with non-stroke cases having more regions with low ECAP (black color on the LAA surface) whereas stroke cases had more white color specially in the cauliflower morphology, representing higher values of ECAP in the representative stroke cases. Overall, qualitatively, representative stroke cases had slightly lower flow into the LAA as compared to the representative non-stroke cases, with both ECAP and OSI showing little differences. Simulation results over the whole cardiac cycle is presented for one case in the Supplementary videos section, representing volume rendering of the velocity magnitude.

## 4. Discussion

In this study, we characterized and compared patient-specific LA and LAA geometrical and hemodynamic parameters of 28 paroxysmal AF patients that had stroke with 27 paroxysmal AF patients that did not have stroke. In this study, we performed detailed blood-flow modeling of the LA in AF patients and correlate them with clinical stroke event. Our hemodynamic analysis showed that stroke group had significantly lower velocity, WSS and higher ECAP in the LAA as compared to the non-stroke group. This suggests that the flow in the LAA for AF patients that had stroke was slow as well as highly oscillatory as compared to AF patients that did not have stroke event. Biologically, this combination of slow and oscillatory flow condition leads to the activation of the endothelial cells at the myocardial wall, starting a coagulation cascade, which begins with local platelet activation followed by thrombus formation mechanisms [30–32]. This thrombus formation mechanism provides a milieu for local clot formation, which could travel to the brain and

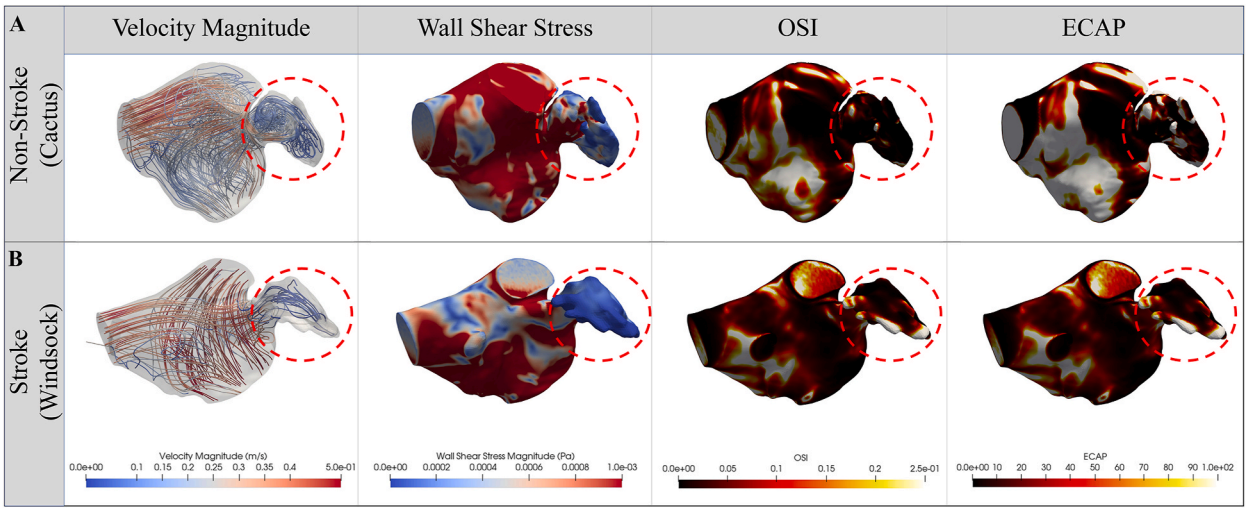


**Fig. 2.** Velocity magnitude, wall shear stress, OSI and ECAP in the left atriums of 1 non-stroke and 1 stroke representative cases from the patient cohort plotted in top and bottom panels. 2A shows the representative cactus morphology case and 2B shows the representative windsock morphology. Red dotted circle in both panels show the LAA. (For interpretation of the references to color in this figure legend, the reader is referred to the Web version of this article.)

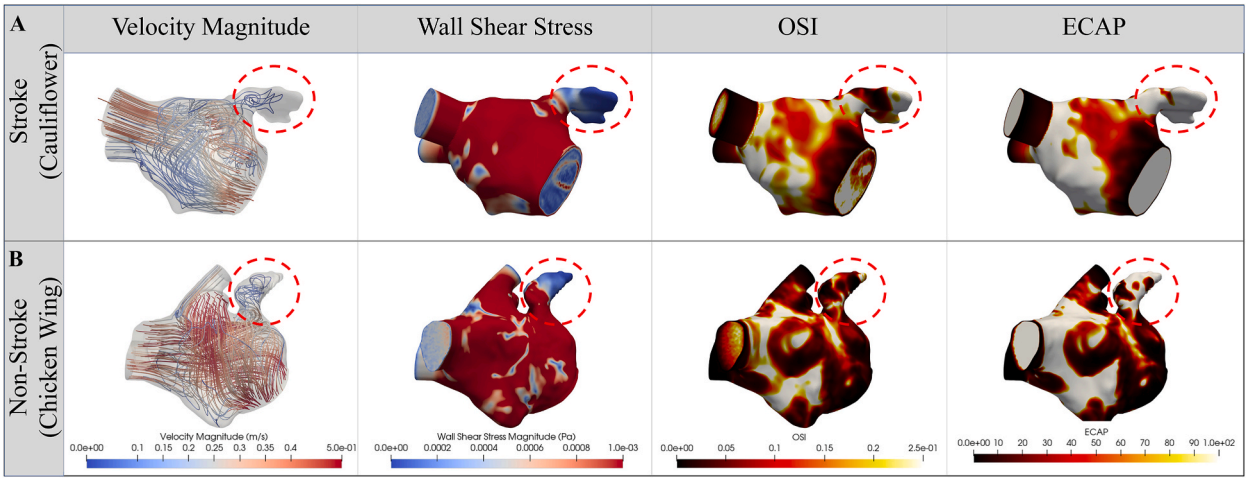


**Fig. 3.** Velocity magnitude, wall shear stress, OSI and ECAP in the left atriums of 1 stroke and 1 non-stroke representative cases from the patient cohort plotted in top and bottom panels. 3A shows the representative cauliflower morphology case and 2B shows the representative chicken wing morphology. Red dotted circle in both panels show the LAA. (For interpretation of the references to color in this figure legend, the reader is referred to the Web version of this article.)

cause stroke. This might explain why slow and oscillatory flow blood-flow conditions in the LAA are associated with stroke for AF patients.

Recently, both computational and clinical studies have emerged that have established correlation between stroke or LAA thrombus as endpoint with low blood-flow in the LA/LAA [8–15,26,33,34]. In one such computational study, Masci et al. showed that different LAA geometries had different blood-flow dynamics which might aid in stratifying stroke risk for such shapes. Here, we have built upon their computational findings of potential hemodynamic differences in the LAA and their association with the clinical outcome of stroke. Consequently, we found that LAA hemodynamics is significantly different for stroke patients as compared to non-stroke ones. Therefore, modeling patient-specific hemodynamics using patients' clinical image improves our understanding of the use of modeling detailed blood-flow activity in the LAA, to potentially improve stroke risk stratification of AF patients using non-invasive *in-silico* approach.

Existing studies have not considered area of PVs while assessing stroke risk for AF patients. Previously, Bonczar suggested that left sided PVs have smaller ostia than the corresponding right-sided PVs, and the inferior PVs ostia are smaller than the superior by meta-analysis [35]. Also, they found that the left common PV ostium size is the largest among all veins analyzed, while the right middle PV ostium is the smallest. We quantified area of all 4 PVs and found that stroke group had bigger LIPV as compared to the non-stroke group. Our results about PVs ostia size were consistent with Bonczars' that right-sided PVs ostia are larger than those of left-sided ostia and superior PVs ostia are larger than those of inferior ostia. We believe that the size of PVs can drastically change the resulting blood-flow coming into the LA and LAA, thus could potentially contribute to the propensity of clot formation in the LA. Thus, size of PVs could also be an important factor in assessing stroke risk for AF patients; future studies will need to confirm our findings. Furthermore, we did not find any association between stroke and LA/LAA geometrical parameters including LAA morphology, contrary to findings of Lee et al. [12,14]. We believe that LA geometrical parameters that we quantified might not be sufficient to accurately capture LAA shape complexity, therefore we did not find a significantly difference between groups. Furthermore, our LAA orifice extraction method was non-clinical and automated, which might be the reason for discrepancy with results of Lee et al. A more detailed and locally resolved LAA geometrical characterization is warranted in future studies that provides rigorous LA, PV and LAA geometrical characterization such as PV angles, which has shown to be correlated to risk of thrombus formation [9,36]. Multiple meta-analysis studies have shown that patients with non-chicken-wing morphology of the LAA had elevated risk of stroke [2,37]. Di Biase also reported that chicken wing LAA morphology are less likely to have an embolic event even after controlling for comorbidities and $CHADS_2$ score [23]. So, we also characterized the LAAs of our patients based on the commonly used 4 morphologies: chicken-wing, cauliflower, cactus and windsock. Our results corroborate with previous clinical findings, with 38.5% of the patients in the non-stroke group had chicken-wing LAA morphology as compared to only 14.8% was in the stroke group. However, there was no statistical significance between the two groups. It may be due to the small number of patients in our cohort. In our previous study, we found that the frequency of cauliflower morphology increased, and the frequency of chicken wing morphology decreased in the non-stroke group [38]. A larger sample size will shed light on the hypothesis that non-chicken wing morphologic type of LAA is correlated with the risk of stroke in paroxysmal AF patients, particularly when accompanied with aberrant LAA hemodynamics.

This study is an example of how CFD simulations can help guide the clinical management of stroke in AF patients. As shown in the hemodynamics results of Figs. 2 and 3, it is seen that the cases with stroke had lower flow in their LAA as depicted by blue velocity streamlines and WSS, and high OSI at the tip of the LAA as depicted by the black color, which is mostly consistent throughout the LAA. Alternatively, for non-stroke cases in Figs. 2 and 3, flow in the LAA is lower than the LA, but it is not slow throughout the LAA as shown in red areas of high WSS in half of the LAA for non-stroke cactus and chicken wing type cases. Detailed hemodynamics like this could be

helpful in stroke-assessment for clinical management of AF patients. However, CFD simulations have their own bottleneck in performing simulations on a large number have associated computational costs. We used generic inlet and outlet boundary conditions in our simulations due to (1) lack of clinical flow data and (2) use simpler CFD flow model to get quick hemodynamic assessment. Even with these assumptions, each simulation took ~8 h to complete on a supercomputer, which are not common in clinical practice and is thus a big bottleneck for CFD simulations translation into the clinic. To tackle this, use of deep learning to predict fluid flow might be a computationally feasible option in the future for clinical implementation.

Our study focused on population-based geometrical and hemodynamic statistics, linking them with stroke as clinical endpoint using bulk parameters. Thus, our study lacked detailed analysis of hemodynamic assessment and visualization for all patients (limited to Figs. 2 and 3 only). This was a big limitation which might result in lack of detailed interpretations and potential generation of novel biological hypothesis. It would be worthwhile to supplement the patient cohort analysis with detailed analysis like that of Masci et al. [33] and Mill et al. [9,16] in future, which might provide better understanding of both clinical and biological pathways in assessing cardiovascular disease management.

This study has a few limitations. First, this is a retrospective proof-of-concept study with a small patient cohort. A larger cohort study needs to be performed to provide substantial diagnostic performance and assess the clinical utility of our analysis. Furthermore, a comparison with the hemodynamics in the LA of healthy subject would be useful to act as a control group. Second, due to the lack of clinical data for the blood-flow through the PVs, we modeled the patient-specific hemodynamics during sinus rhythm with blood-flow through the PVs interpolated from the literature due to the lack of clinical data to model the blood-flow during AF event. Additionally, an unvalidated method of SDF algorithm was used to identify and isolate the LAA orifice, which could introduce some inconsistencies in calculations across patients. Further validation of the accuracy of the SDF for LAA isolation is required in future studies. Furthermore, our simulations also assumed rigid LA wall, which does not represent the physiological conditions of the LA during sinus-rhythm, and we considered the second LA contraction peak based on interpolated velocity values instead of pressure outlet values, which would be more physiologically accurate. Future studies could use a pressure condition at the outlet as described by Park et al. [39] as well as compare simulation results of rigid LA wall against wall-motion to verify the results. Third, the semi-automated methodology for segmentation to obtain LA geometry could be susceptible to the quality of the CT image. However, a single experienced operator performed the segmentation to minimize the possibility of subjectivity in obtaining the 3D LA shape. To make this technique completely automated and objective, artificial intelligence could be used for segmentation of cardiac CT images. This would enable reproducible assessment, thus enabling its application on a much larger population risk stratification study. Our CFD methodology also carries few limitations such as rigid LA wall assumption, which is not physiologic. Furthermore, due to the slow flow in the LAA, flow might be non-Newtonian in nature, but our simulation assumed Newtonian flow throughout the flow domain. Finally, our simulations were performed assuming same heart rate for all patients, which do not account for the inter and intra-patient heart rate variations which will modify their resulting blood-flow.

## Sources of funding

This work was supported by American Heart Association Grant # 830952 to NP, National Institutes of Health Grant no. U01-HL141074 to NAT and the Korean Society of Cardiology Grant no. 202003-06 to HP.

## Data availability statement

The processed data including LA geometrical and CFD velocity field data is available upon suitable request, after institutional approval.

## CRediT authorship contribution statement

**Nikhil Paliwal:** Writing – original draft, Methodology, Conceptualization. **Hwan-Cheol Park:** Writing – review & editing, Data curation, Conceptualization. **Yuncong Mao:** Software, Formal analysis. **Su Jin Hong:** Data curation. **Yonggu Lee:** Data curation. **David D. Spragg:** Writing – original draft, Supervision. **Hugh Calkins:** Writing – original draft, Supervision. **Natalia A. Trayanova:** Writing – review & editing, Writing – original draft, Supervision, Methodology, Conceptualization.

## Declaration of competing interest

The authors declare that they have no known competing financial interests or personal relationships that could have appeared to influence the work reported in this paper.

## Appendix A. Supplementary data

Supplementary data to this article can be found online at https://doi.org/10.1016/j.heliyon.2024.e26858.

## References


[1] J. Andrade, et al., The clinical profile and pathophysiology of atrial fibrillation: relationships among clinical features, epidemiology, and mechanisms, Circ. Res. 114 (9) (2014) 1453–1468.
[2] M. Alkhouli, P.A. Friedman, Ischemic stroke risk in patients with nonvalvular atrial fibrillation: JACC review topic of the Week, J. Am. Coll. Cardiol. 74 (24) (2019) 3050–3065.
[3] J.Y. Chen, et al., CHADS2 versus CHA2DS2-VASc score in assessing the stroke and thromboembolism risk stratification in patients with atrial fibrillation: a systematic review and meta-analysis, J Geriatr Cardiol 10 (3) (2013) 258–266.
[4] G.R. Quinn, et al., Wide variation in reported rates of stroke across cohorts of patients with atrial fibrillation, Circulation 135 (3) (2017) 208–219.
[5] T.F. Chao, et al., Validation of a modified CHA2DS2-VASc score for stroke risk stratification in Asian patients with atrial fibrillation: a nationwide cohort study, Stroke 47 (10) (2016) 2462–2469.
[6] S. Yaghi, H. Kamel, Stratifying stroke risk in atrial fibrillation: beyond clinical risk scores, Stroke 48 (10) (2017) 2665–2670.
[7] S. Nattel, B. Burstein, D. Dobrev, Atrial remodeling and atrial fibrillation: mechanisms and implications, Circ Arrhythm Electrophysiol 1 (1) (2008) 62–73.
[8] M. Markl, et al., Left atrial 4-dimensional flow magnetic resonance imaging: stasis and velocity mapping in patients with atrial fibrillation, Invest. Radiol. 51 (3) (2016) 147–154.
[9] J. Mill, et al., In-silico analysis of the influence of pulmonary vein configuration on left atrial haemodynamics and thrombus formation in a large cohort, in: International Conference on Functional Imaging and Modeling of the Heart, Springer, 2021.
[10] B.T. Costello, et al., Measuring atrial stasis during sinus rhythm in patients with paroxysmal atrial fibrillation using 4 Dimensional flow imaging: 4D flow imaging of atrial stasis, Int. J. Cardiol. 315 (2020) 45–50.
[11] M. García-Villalba, et al., Demonstration of patient-specific simulations to assess left atrial appendage thrombogenesis risk, Front. Physiol. 12 (2021) 596596.
[12] J.M. Lee, et al., Impact of increased orifice size and decreased flow velocity of left atrial appendage on stroke in nonvalvular atrial fibrillation, Am. J. Cardiol. 113 (6) (2014) 963–969.
[13] T. Takada, et al., Blood flow in the left atrial appendage and embolic stroke in nonvalvular atrial fibrillation, Eur. Neurol. 46 (3) (2001) 148–152.
[14] Y. Lee, et al., Comparison of morphologic features and flow velocity of the left atrial appendage among patients with atrial fibrillation alone, transient ischemic attack, and cardioembolic stroke, Am. J. Cardiol. 119 (10) (2017) 1596–1604.
[15] M.E. Goldman, et al., Pathophysiologic correlates of thromboembolism in nonvalvular atrial fibrillation: I. Reduced flow velocity in the left atrial appendage (The Stroke Prevention in Atrial Fibrillation [SPAF-III] study), J. Am. Soc. Echocardiogr. 12 (12) (1999) 1080–1087.
[16] J. Mill, et al., Patient-specific flow simulation analysis to predict device-related thrombosis in left atrial appendage occluders, REC (Rev. Esp. Cardiol.): Interventional Cardiology. 3 (4) (2021) 278–285, 2021.
[17] M.I. Pons, et al., Joint analysis of morphological parameters and in silico haemodynamics of the left atrial appendage for thrombogenic risk assessment, J. Intervent. Cardiol. (2022) 2022.
[18] A. Gonzalo, et al., Non-Newtonian blood rheology impacts left atrial stasis in patient-specific simulations, International Journal for Numerical Methods in Biomedical Engineering (2022) e3597.
[19] D. Vella, et al., Effect of the alterations in contractility and morphology produced by atrial fibrillation on the thrombosis potential of the left atrial appendage, Front. Bioeng. Biotechnol. 9 (2021) 586041.
[20] G.M. Bosi, et al., Computational fluid dynamic analysis of the left atrial appendage to predict thrombosis risk, Frontiers in cardiovascular medicine 5 (2018) 34.
[21] G. Musotto, et al., The role of patient specific morphological features of the left atrial appendage on the thromboembolic risk under atrial fibrillation, Frontiers in Cardiovascular Medicine (2022) 1830.
[22] Y. Lee, et al., Comparison of morphologic features and flow velocity of the left atrial appendage among patients with atrial fibrillation alone, transient ischemic attack, and cardioembolic stroke, Am. J. Cardiol. 119 (10) (2017) 1596–1604.
[23] L. Di Biase, et al., Does the left atrial appendage morphology correlate with the risk of stroke in patients with atrial fibrillation? Results from a multicenter study, J. Am. Coll. Cardiol. 60 (6) (2012) 531–538.
[24] H.C. Park, et al., Left atrial appendage: morphology and function in patients with paroxysmal and persistent atrial fibrillation, Int. J. Cardiovasc. Imag. 29 (4) (2013) 935–944.
[25] P.A. Yushkevich, et al., User-guided 3D active contour segmentation of anatomical structures: significantly improved efficiency and reliability, Neuroimage 31 (3) (2006) 1116–1128.
[26] N. Paliwal, et al., Presence of left atrial fibrosis may contribute to aberrant hemodynamics and increased risk of stroke in atrial fibrillation patients, Front. Physiol. 12 (2021) 657452.
[27] N. Paliwal, et al., Outcome prediction of intracranial aneurysm treatment by flow diverters using machine learning, Neurosurgical focus 45 (5) (2018) E7.
[28] N. Paliwal, et al., Methodology for computational fluid dynamic validation for medical use: application to intracranial aneurysm, Journal of biomechanical engineering 139 (12) (2017) 121004.
[29] J. Ahrens, B. Geveci, C. Law, Paraview: an end-user tool for large data visualization, The Visualization Handbook (2005) 717.
[30] M. Koupenova, et al., Thrombosis and platelets: an update, Eur. Heart J. 38 (11) (2017) 785–791.
[31] T. Torisu, et al., Autophagy regulates endothelial cell processing, maturation and secretion of von Willebrand factor, Nat. Med. 19 (10) (2013) 1281–1287.
[32] N. Mackman, New insights into the mechanisms of venous thrombosis, J. Clin. Invest. 122 (7) (2012) 2331–2336.
[33] A. Masci, et al., The impact of left atrium appendage morphology on stroke risk assessment in atrial fibrillation: a computational fluid dynamics study, Front. Physiol. (2019) 1–11.
[34] T. Otani, et al., A computational framework for personalized blood flow analysis in the human left atrium, Ann. Biomed. Eng. (2016) 3284–3294.
[35] M. Bonczar, et al., Variations in human pulmonary vein ostia morphology: a systematic review with meta-analysis, Clin. Anat. 35 (7) (2022) 906–926.
[36] E.T. Bieging, et al., Statistical shape analysis of the left atrial appendage predicts stroke in atrial fibrillation, Int. J. Cardiovasc. Imag. 37 (8) (2021) 2521–2527.
[37] F. Lupercio, et al., Left atrial appendage morphology assessment for risk stratification of embolic stroke in patients with atrial fibrillation: a meta-analysis, Heart Rhythm 13 (7) (2016) 1402–1409.
[38] W.K. Jeong, et al., Volume and morphology of left atrial appendage as determinants of stroke subtype in patients with atrial fibrillation, Heart Rhythm 13 (4) (2016) 820–827.
[39] J. Park, et al., High left atrial pressures are associated with advanced electroanatomical remodeling of left atrium and independent predictors for clinical recurrence of atrial fibrillation after catheter ablation, Heart Rhythm 11 (6) (2014) 953–960.